ACSNANO
www.acsnano.org
ARTICLE

Vesicle Geometries Enabled by Dynamically Trapped States

Jiaye Su,[†,⊥,¶] Zhenwei Yao,[†,¶] and Monica Olvera de la Cruz[*,†,‡,§,∥]

[†]Department of Materials Science and Engineering, [‡]Department of Chemistry, [§]Department of Chemical and Biological Engineering, and [∥]Department of Physics, Northwestern University, Evanston, Illinois 60208-3108, United States

[⊥]Department of Applied Physics, Nanjing University of Science and Technology, Nanjing, Jiangsu 210094, China

ABSTRACT: **Understanding and controlling vesicle shapes is a fundamental challenge in biophysics and materials design. In this paper, we design dynamic protocols for enlarging the shape space of both fluid and crystalline vesicles beyond the equilibrium zone. By removing water from within the vesicle at different rates, we numerically produced a series of dynamically trapped stable vesicle shapes for both fluid and crystalline vesicles in a highly controllable fashion. In crystalline vesicles that are continuously dehydrated, simulations show the initial appearance of small flat areas over the surface of the vesicles that ultimately merge to form fewer flat faces. In this way, the vesicles transform from a fullerene-like shape into various faceted polyhedrons. We perform analytical elasticity analysis to show that these salient features are attributable to the crystalline nature of the vesicle. The potential to use dynamic protocols, such as those used in this study, to engineer vesicle shape transformations is helpful for exploiting the richness of vesicle geometries for desired applications.**

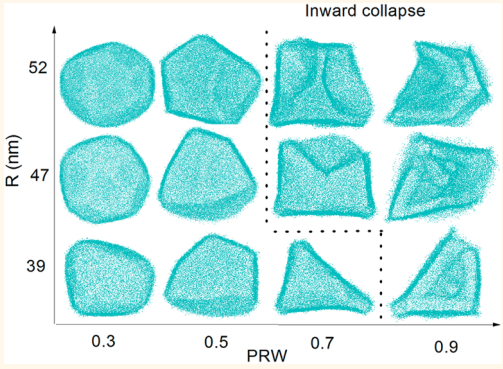

KEYWORDS: *vesicles, molecular dynamics, shapes, polyhedron, dynamic protocol*

The spontaneous formation of closed vesicles from microscopic units in aqueous solutions is a fundamental process in biology and materials science,[1,2] occurring in phenomena ranging from the assembly of viruses[3] to the fabrication of various cage-like structures in materials design.[4] The rich morphologies of the resulting vesicles create a multitude of possibilities for functionalization in diverse fields, notably in drug delivery,[5] encapsulation,[6] and the realization of relevant biological processes like endocytosis *via* the shape transformations of cell membranes.[1] Understanding the underlying principles of vesicle organization is fundamental to solving a host of problems in materials geometry and biology. For example, deciphering the self-assembly of viral shells from capsid proteins may ultimately lead to the cure of many viral diseases.[3] The synthesis of fluid vesicles from various surfactant molecules has been extensively studied experimentally[7−13] and theoretically,[14] and the governing force behind such vesicle formation is believed to be the amphiphilic nature of the constituting molecules. In addition, crystalline vesicles, occurring in both natural and artificial systems, represent another important class of vesicles that can exhibit morphologies not found in fluid vesicles.[15,16]

The equilibrium shapes of both fluid and crystalline vesicles have been studied using several theoretical models, including the bilayer coupling model,[17] the spontaneous curvature model,[17] and the area-difference elasticity model.[18] In addition to analytical models and experiments, computer simulations based on coarse-grained molecular dynamics (CGMD)[19−21] and dissipative particle dynamics[22] can provide detailed information about the vesicle formation process. These tools can help us derive valuable insights into the physics of vesicles. The equilibrium vesicle shape space is significantly expanded by introducing extra structures into vesicle systems, such as embedding in-plane orders,[23−25] inclusion of electric charges,[26,27] and introduction of multiple components,[16,28] resulting in geometries not found in structureless vesicles. However, the vesicle shape space beyond the equilibrium zone has not been fully explored through designed, controllable dynamic protocols.

The objective of this work is to design a controllable dynamic protocol for enlarging the vesicle shape space beyond the equilibrium zone, in both fluid and crystalline vesicle systems. We employ computer simulations based on the CGMD,[19−21] as well as elasticity analysis. Specifically, we design a model system composed of ionic amphiphiles [−1 palmitic acid (C_{15}−COOH) and +3 trilysine (C_{16}−K_3)] and water molecules. The spontaneous formation of closed bilayer vesicles from the ionic amphiphilic molecules is numerically observed. Simulations capture the permeation of water molecules through the membrane and the consequent vesicle shape transformations.

Received: November 5, 2015
Accepted: January 21, 2016
Published: January 21, 2016

DOI: 10.1021/acsnano.5b06991
ACS Nano 2016, 10, 2287−2294

By controlling the rate of dehydration from within the vesicle, mimicking the outward permeation of water molecules at different rates, we numerically obtained a variety of shapes. For fluid and crystalline vesicles, we found a distinct series of shapes by utilizing different dehydration rates. Notably, and in sharp contrast with fluid vesicles, simulations revealed that the dynamically driven deformations of the originally spherical crystalline vesicles followed a unified pattern regardless of size. The surface areas that initially emerged as small flat areas coalesced to form larger flat faces, and consequently, the entire vesicle transformed from a fullerene-like shape into various faceted polyhedrons. The deformation mechanism provided by the collective dynamics of the initially small flat areas is reported here for the first time. The trapped states of both fluid and crystalline vesicles that result from our dynamic protocols turned out to be very stable at room temperature, suggesting that they belong to a class of metastable states sitting deep in the energy valleys. We propose an analytical elasticity model to account for the appearance of the small flat areas on the crystalline vesicles. This model is a key to understanding these areas' eventual merge, reshaping the originally spherical vesicles into polyhedrons. This study could open new possibilities for obtaining vesicle geometries not accessible (or not sufficiently efficient) by spontaneous equilibration processes.

RESULTS AND DISCUSSION

We first considered the case of fluid vesicles. Figure 1a shows the mean-squared radius of gyration $\langle R_g^2 \rangle$ of the fluid vesicle, a measure of its shape, as a function of the percentage of removed water (PRW), as well as some typical shape snapshots. The radius of gyration is calculated from the positions of the lipid tail terminals. Bifurcation of the vesicle radius using the protocols *I* and *M* occurs when the PRW exceeds about 40%, as can be seen in Figure 1a. Dehydration leads to reduction of the vesicle volume. Consequently, the vesicle has to change its shape to conserve surface area. This volume-driven shape deformation mechanism applied to both fluid and crystalline vesicles in our study. Notably, the *I* protocol leads to a pronounced non-monotonous variation of $\langle R_g^2 \rangle$. Closer examination showed that the vesicle experienced a morphological transition from sphere to elliptocyte (or prolate), cigar (or dumbbell), and finally to a curved disc with the increase of PRW, as shown in the Figure 1a insets. In sharp contrast, Figure 1a also shows that the overall size of the obtained vesicle shapes after bifurcation was significantly smaller in protocol *M* than in protocol *I*. Therefore, protocol *M* leads to a distinct series of shapes. Specifically, by directly removing half of the water within the vesicle, nearly half of the vesicle collapsed to form a whistle-like object, while the vesicle well maintained an elliptocyte shape at PRW = 30%. The *M* protocol even led to the inward collapse of the vesicle at larger PRW, including the shape resembling a stomatocyte obtained at PRW = 70%, and the inward budding phenomenon at PRW = 90%, as shown in the insets of Figure 1a. Some of these shapes found in fluid vesicles have also been reported in experiment,[13] theory,[17,18] and MD simulation, based on implicit solvent and a one-particle-thick membrane model,[21] though this was under distinct constraint conditions.

Simulations showed that fluid vesicles obtained using both protocols are stable, at least over the entire simulation run time of up to 50 ns. Energy analysis in Figure 1b shows that the shapes obtained from protocol *I* have much higher energy than those caused by protocol *M* at high PRW, where the potential

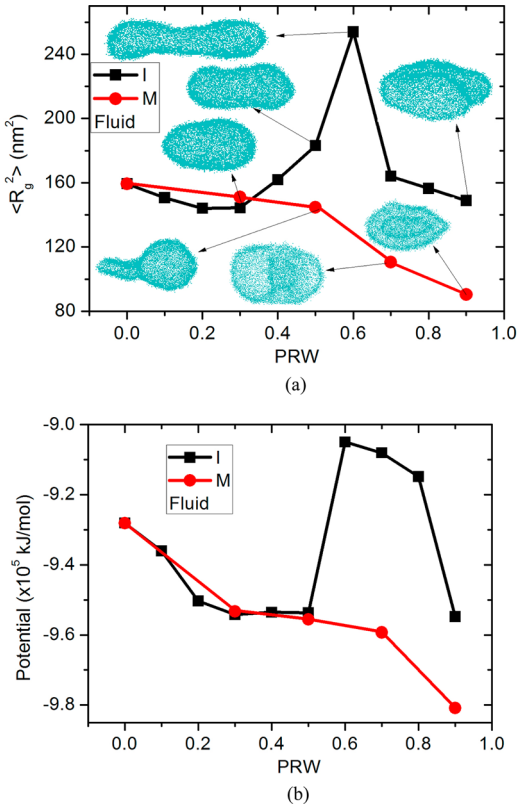

Figure 1. (a) Mean-squared radius of gyration and (b) potential energy of a fluid vesicle as a function of the percentage of removed water. The two dynamic protocols, *I* and *M*, lead to bifurcation in the shape evolution. Along the black curve (protocol *I*), the vesicle experiences transformations from elliptocyte, elliptocyte, elongated elliptocyte, to curved bilayer disc. Along the red curve (protocol *M*), the typical shapes are elliptocyte, whistle, stomatocyte, and inwardly buckled stomatocyte. At PRW = 30%, the two protocols result in similar shapes but with slightly different size and potential. The error bars (around 1%) are even smaller than the data symbols and are not shown for clarity. The outer diameter of the vesicle is 28 nm.

energy contains the Lennard-Jones and Coulomb interactions between all the lipid particles. It suggests that these shapes belong to the metastable states at the bottom of sufficiently deep energy valleys. The employed dynamic protocols are essential for exploring the rich metastable states in the shape space of the vesicle. While it is not uncommon to encounter metastable states in generic many-body systems,[29] it is a challenge to realize specific metastable states in a controllable fashion. It seems that, in the context of our vesicle system, dynamically controlling the vesicle volume provides a promising protocol for achieving this goal. We will illustrate this point further in our study of crystalline vesicles.

In comparison with fluid vesicles, crystalline vesicles can exhibit various polyhedral shapes, as shown in both theory,[15,16] experiments[30] and our own previous simulations.[31] However, it remains a challenge to obtain faceted crystalline vesicles in a controllable fashion. Our proposed methodology, based on the protocol of dynamically varying the vesicle volume, seems promising for creating desired faceted shapes. Figure 2a shows the mean-squared radius of gyration of the crystalline vesicles as a function of the PRW. We see that the shape bifurcation due to the distinct dynamic protocols also exists for the crystalline vesicle, occurring at about PRW = 50%. Standard error bars are

DOI: 10.1021/acsnano.5b06991
ACS Nano 2016, 10, 2287–2294

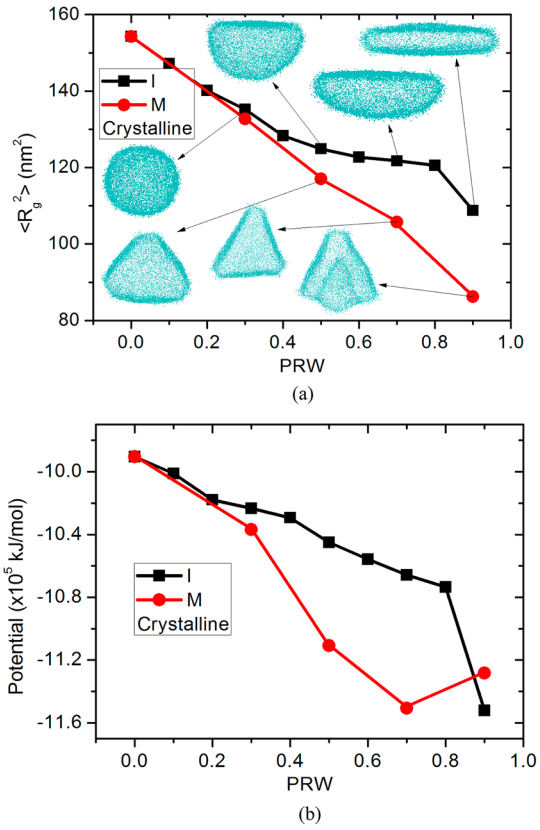

Figure 2. (a) Mean-squared radius of gyration and (b) potential energy of a given crystalline vesicle as a function of the percentage of removed water. The two dynamic protocols, *I* and *M*, lead to bifurcation in the shape evolution. Along the black curve (protocol *I*), the vesicle experiences transformations from sphere, buckled half-sphere, oblate half-sphere, to disc. Along the red curve (protocol *M*), the typical shapes are sphere, tetrahedron with a rounded face, tetrahedron, and inwardly buckled tetrahedron. When PRW = 30%, the two protocols result in similar shapes but with slightly different size and potential. The error bars (around 1%) are smaller than the data symbols and are not shown for clarity. The outer diameter of the vesicle is 28 nm.

estimated by the last 50 ns (50 samples) MD trajectory. It turns out that all of the error bars in the curves of vesicle size and energy are within about 1%. This observation confirms that the vesicle shape evolution is a robust process that is under the full control of the adopted dynamic protocols. In comparison with fluid vesicles, a salient feature of the crystalline vesicle deformation is that the initial deformation occurs locally, resulting in a flattened face whose size increases with PRW. This local deformation is closely related to the crystalline nature of the vesicle that inhibits the even distribution of curvature around the surface. In protocol *I*, the vesicle approaches the shape of a half-sphere with a flat crystalline face at PRW = 50%, and it evolves toward a flattened disk at PRW = 90%, as shown in Figure 2a. In contrast, Figure 2a shows that protocol *M* can generate smaller vesicles with distinct shapes. This is similar to the fluid vesicle case. With PRWs as large as 30%, the vesicle remains in a perfect spherical shape, as the result of competition between surface tension and the strain and bending energies according to our elasticity analysis, which will be discussed later in detail. When PRW = 50%, the vesicle forms a tetrahedron with rounded edges and vertices that are not found in protocol *I* (see Figure 2a). The formation of the tetrahedral shape seems insensitive to the ionization level of the palmitic acid molecules; our simulations show that the vesicle maintains the tetrahedral shape by changing the ionization of the palmitic acid molecules from 30 to 50%. This suggests that the dynamic protocol utilized plays a decisive role in shaping the vesicle. When PRW = 70% in the *M* protocol, the tetrahedral vesicle becomes even more faceted with four perfectly flat faces. With further reduction in volume, we numerically observe inward buckling at one of the four faces in the tetrahedral vesicle, as shown in Figure 2a (PRW = 90%). Note that the *M* protocol generally leads to a reduction in system energy alongside an increase of PRW for both fluid and crystalline vesicles (see the red curves in Figure 1b and Figure 2b). The slight increase of energy in the deformed crystalline vesicle when PRW = 90%, observed in Figure 2b, may be caused by repulsion between the bilayers in the inward collapse event.

We next studied how vesicle size influenced the kinetically driven shape transformation. In cases of larger vesicles with outer diameters of 39, 47, and 52 nm, Figure 3 demonstrates

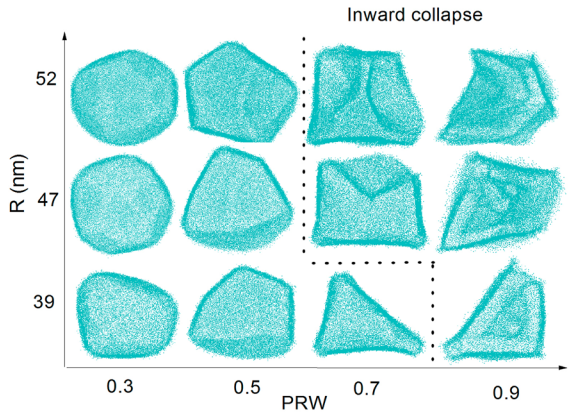

Figure 3. Shape evolution of crystalline vesicles with different sizes under protocol *M*. The deformation of the vesicles follows a pattern with the increase of the percentage of removed water: the initially emergent small flat areas over the surface (at PRW = 30%) coalesce to form a few larger flat faces (at PRW = 50%), and the entire vesicle transforms from a fullerene-like shape to various faceted polyhedrons (see the shapes at PRW = 50%). These polyhedrons are inwardly collapsed with the further removal of water. The dotted line indicates the shape transition of the inward collapse.

how the *M* protocol drives the shape evolution of these vesicles at levels of PRW ranging from 30 to 90%. We see that larger vesicles are easier to deform. For example, when PRW = 30%, these larger vesicles have obviously deviated from the spherical shape assumed by smaller vesicles at the same level of PRW. Remarkably, flat areas, absent in smaller vesicles, emerge on the surface of the larger vesicles. The number of flat areas are 3, 10, and 18 for *R* = 39, 47, and 52 nm and PRW = 0.3, respectively. The latter two are fullerene-like shapes. Limited available free space prevents these flat areas from growing. Simulations capture the coalescence of these small flat areas into few larger ones that ultimately form various polyhedrons as shown for PRW = 50 and 70% in Figure 3. These polyhedrons stably exist during the entire simulation runs of the last 50 ns, and further reduction of volume drives their collapse, starting from the flat faces (PRW = 70 and 90%). A dotted line distinguishes the inwardly collapsed vesicle shapes in Figure 3. It seems that a larger vesicle is easier to collapse with the increase of PRW. To

DOI: 10.1021/acsnano.5b06991
ACS Nano 2016, 10, 2287−2294

conclude, the shape transformation of the crystalline vesicle, regardless of its size, follows a specific pattern. The initially formed small flat areas, as well as their coalescence, are crucial to understanding the ensuing formation of various polyhedrons, whose number of faces is determined by the vesicle size.

The shapes listed in Figure 3 were obtained after sufficiently long MD runs. We run independent MD simulations for some of these cases and ultimately obtained similar shapes. For example, starting from two distinct initial states, the vesicles with a radius of 28 nm at T = 300 K and PRW = 0.5 uniformly evolve toward barely distinguishable tetrahedral shapes. We also increased the degree of ionization (up to 50%) with counterions (Na^+). It turned out that the 50% ionization condition also exhibits a similar tetrahedron shape but with more flat areas and sharper angles for the ionization-dependent electrostatic interactions between lipids. For larger vesicles, it seems that the number and specific position of the flat areas over the vesicles are weakly dependent on the initial conformations. For example, for the case of R = 47 nm, T = 300 K, and PRW = 0.5, we count out a similar number of flat areas (around 8−9) over the same vesicle for two independent simulation runs. The resultant shapes of these larger vesicles, however, are still uniformly polyhedral like the smaller vesicles.

In contrast with fluid vesicles, crystalline vesicles preserve the spherical geometry well, until the amount of removed water exceeds some critical value. Among the subsequent symmetry-breaking deformations, the appearance of the flat areas scattered over the vesicle surface is of particular interest. Understanding the emergence of these areas constitutes a foundation for explaining the ensuing and more sophisticated tetrahedral shape. In the following, we propose an elastic free energy and perform perturbation calculations to analyze these salient features of crystalline vesicles. The crystalline vesicle is modeled as a continuum elastic medium. The elasticity of the crystalline vesicles is explicitly exhibited in the vesicle shape fluctuations observed in simulations. The continuum representation of the vesicle provides an analytically tractable tool to calculate its shape deformation; the crystalline structure and the topological defect structure therein are smeared out.[32] A few phenomenological elastic parameters encode the microscopic information about the interactions between the elementary units composing the vesicle.

The free energy cost for the deformation $\vec{u}(\theta, \phi)$ of an originally spherical elastic vesicle of radius R is

$$F = F_s + F_b + \sigma(A - A_0) + \gamma(V - V_w) \tag{1}$$

where the stretching energy $F_s = \frac{1}{2}\int dA(2\mu u_{ij}^2 + \lambda u_{kk}^2)$ and the bending energy $F_b = \frac{\kappa}{2}\int dA(H - H_0)$. Here, μ and λ are the Lamé coefficients.[33] These phenomenological elastic moduli can be determined experimentally by scattering techniques.[34] The elastic moduli of the specific vesicles investigated in this work are not experimentally measured yet.[31,36] Determining their values is a very important but nontrivial problem. For example, the bending rigidity κ can be renormalized by thermal fluctuations, and discretized models of a membrane show that its value is dependent on the shape of the membrane.[35] Furthermore, the electrostatic interaction can make a long-range contribution to the elastic moduli. We therefore study the deformation pattern on the crystalline vesicle over a wide range of the values for the elastic moduli. The strain tensor $u_{ij}^2 = u_{ij}u^{ij}$, $u_{kk}^2 = (u_k^k)^2$, where u_k^k is the trace of the strain tensor u_{ij} (summation convention is applied). The mean curvature $H = \frac{1}{2}\left(\frac{1}{R_1} + \frac{1}{R_2}\right)$ and $H_0 = 1/R$. $V_w = V_0 - \delta V$, where δV is the volume of removed water; $V_0 = \frac{4\pi}{3}R^3$; $A_0 = 4\pi R^2$; κ is the bending rigidity. The last two terms in eq 1 are due to the conservation of area and volume, respectively. Here, we ignore the contribution from the inevitable topological defects in spherical crystals in the perturbation calculation.[32] For axis-symmetric deformation of $\vec{u} = u_r(\theta)\vec{e}_r$ with $u_\theta, u_\phi \ll u_r$, we have[37]

$$\begin{aligned} F[u_r(\theta)] = {} & 2(\mu + \lambda)\int dA\left(\frac{u_r(\theta)}{R}\right)^2 \\ & + \frac{\kappa}{2R^4}\int dA\left[u_r(\theta) + \frac{1}{2}u_r''(\theta)\right]^2 \\ & + \sigma\int dA\left[\frac{2u_r(\theta)}{R} + \frac{u_r'(\theta)^2}{2R^2} + \left(\frac{u_r(\theta)}{R}\right)^2\right] \\ & + \gamma\left[\delta V + \int dA\left(u_r(\theta) + \frac{u_r(\theta)^2}{R}\right)\right] \end{aligned} \tag{2}$$

where the integration is over the unperturbed sphere of radius R. Note that the u_r term in F_b results from the spherical geometry of the vesicle; this term vanishes in the large R limit. The shape equation in the limit of $\Gamma_\sigma = \frac{2\pi\sigma R^2}{4\pi(\mu+\lambda)R^2 + \kappa} \to 0$ is $\frac{1}{4}u_r^{(4)}(\theta) + u_r''(\theta) + (1 + \Gamma_\mu)u_r(\theta) = 0$, where $\Gamma_\mu = 4(\mu + \lambda)R^2/\kappa$ reflects the competition between in-plane strain and bending. The volume and area constraints, which may be explicitly imposed, are relaxed in the derivation for the shape equation. The existence of the high-order term $u_r^{(4)}$ implies the rich stable (or metastable) shapes that a crystalline vesicle can exhibit.

Equation 2 provides the theoretical basis for analyzing the stability of the vesicle with removal of water and the featured resulting deformation patterns. We first analyze the well-preserved spherical geometry of the vesicle with the initial removal of water. The change of the free energy in the uniform shrinking of the vesicle is obtained by equating $u_r = -a$ ($a > 0$):

$$F[a] = a[(1 + \Gamma_\sigma)a - 2R\Gamma_\sigma] \tag{3}$$

where the value for a is determined by the amount of removed water for the volume conservation. Specifically, $a = \frac{R}{2}\left(1 - \sqrt{1 - \frac{\delta V}{\pi R^3}}\right) = \frac{\delta V}{4\pi R^2} + o(\delta V^2)$. Equation 3 shows the competition between the decreasing surface energy (the second term) and the increasing strain/bending energy $F_s + F_b$ (the first term). Consequently, the free energy of the system becomes positive for $a > 2R\Gamma_\sigma/(1 + \Gamma_\sigma)$, which provides a plausible criterion to predict the vesicle instability at sufficiently large shrinking. In term of the amount of removed water δV, this instability condition becomes $\delta V > \delta V_c = 8\pi R^3\frac{\Gamma_\sigma}{1 + \Gamma_\sigma}$. This equation may be used to estimate the relevant materials parameters directly from the instability of the vesicle. We proceed to analyze the origin of the emergent flat areas over the vesicle surface in simulations. We propose an ansatz shape with three indefinite parameters:

DOI: 10.1021/acsnano.5b06991
ACS Nano 2016, 10, 2287−2294

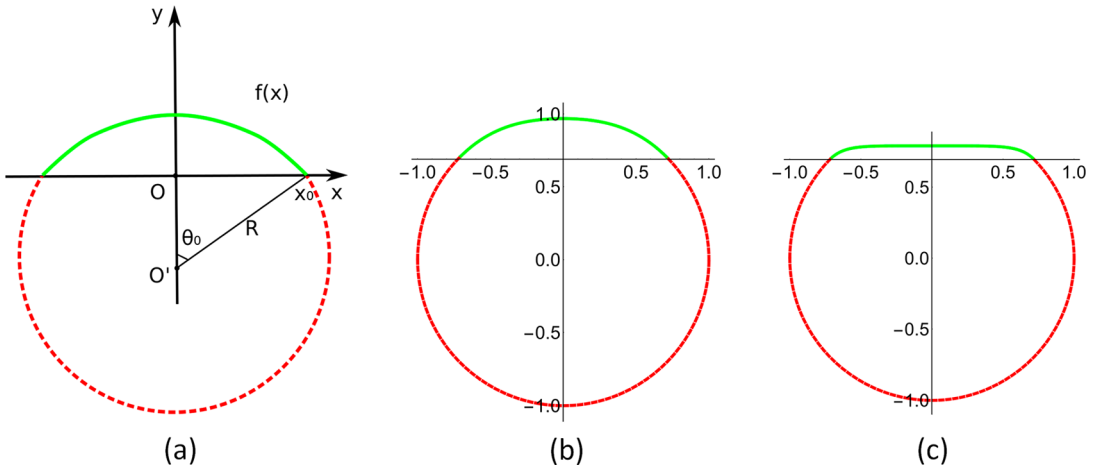

Figure 4. Plot of the ansatz shape $f(x)$ that is proposed to analyze the deformation of the vesicle. The expression for $f(x)$ is given in the text. (a) Coordinate system where the function $f(x)$ is plotted as a solid green curve. (b,c) Ansatz shape $f(x;\alpha)$ can well represent both curved and flat areas; α = 1 and 5 in (a) and (b), respectively; θ_0 = 0.8; R = 1.

$$f(x;\ \alpha,\ \beta,\ x_0) = \beta\left[1 - \left(\frac{x}{x_0}\right)^2 e^{\alpha(x-x_0)}\right] \tag{4}$$

Such an ansatz shape is able to capture both curved and flat areas over the vesicle, as shown in Figure 4. The coordinate system is shown in Figure 4a. The derivative of $f(x)$ at $x = 0$ automatically vanishes. To make a smooth connection at $x = x_0$ with the circular curve, we require $\left(\frac{df(x)}{dx}\right)_{x=x_0} = -\tan\theta_0$, which leads to the relation between β and α, $\beta = \frac{\tan\theta_0 x_0}{2+\alpha x_0}$. The volume conservation condition can be implemented by varying x_0. To examine the influence of the crystalline structure on the profile of the deformed vesicle, we consider the case in which the strain energy dominates over the surface tension $\left(\Gamma_\sigma = \frac{2\pi\sigma R^2}{4\pi(\mu+\lambda)R^2+\kappa} \to 0\right)$. Figure 5 shows that the flattened

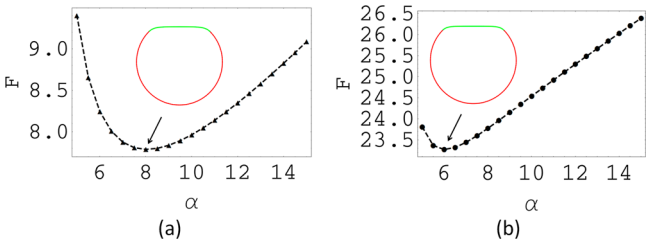

Figure 5. Free energy *versus* the parameter α that characterizes the shape of the vesicle. $\Gamma_\mu = 10^{-3}$ and 10^3 in (a) and (b), respectively. Insets show the corresponding vesicle shapes at the optimal values for α; R = 1; δV = 5% V_0. The volume conservation has been imposed.

configurations are always preferred in a wide range of the value for Γ_μ. Due to the lack of the experimental data for the elastic moduli of the vesicle, here we specify the value for Γ_μ covering six magnitudes from 10^{-3} to 10^3. This result suggests that the flattened buckling mode may be a generic feature of crystalline vesicles subject to dynamic protocols exemplified by the *M* and *I* protocols investigated in this work.

The schematic phase diagram of both fluid and crystalline vesicles in Figure 6 summarizes their controllable shape transformations in the *M* and *I* protocols. The bifurcation of

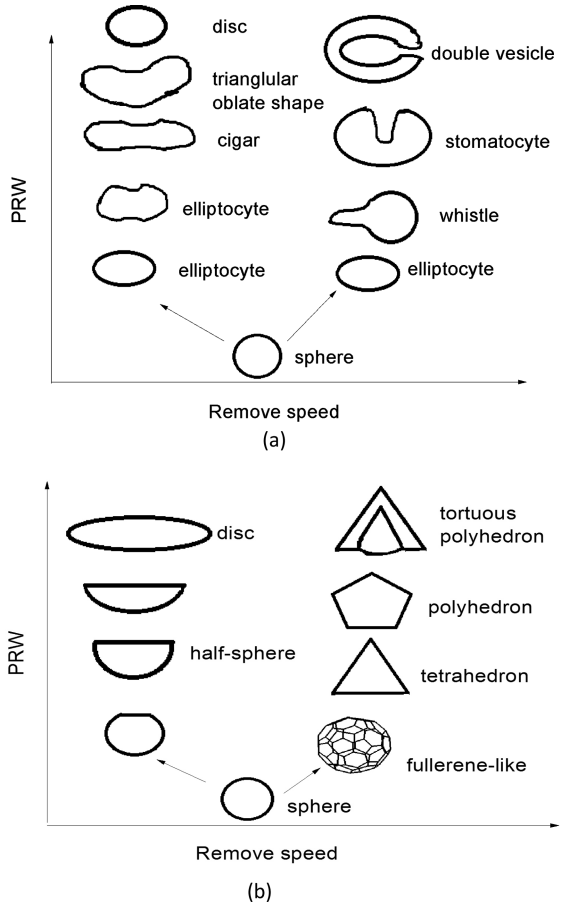

Figure 6. Phase diagram of (a) fluid and (b) crystalline vesicles as a function of PRW and removing speed. The shapes in the left and right columns are generated under the protocol *I* and *M*, respectively.

their shape evolution in these two protocols is clearly seen. Of particular interest, in contrast to fluid vesicles, the crystalline vesicles under protocol *I* can exhibit the remarkable faceting phenomenon that is crucial for formation of polyhedrons; the associated pattern in the shape deformation discussed in the previous sections is schematically plotted in Figure 6. It is

DOI: 10.1021/acsnano.5b06991
ACS Nano 2016, 10, 2287−2294

important to note that the series of shapes obtained through the dynamic protocols are controllably generated. These shapes should belong to the metastable states of the vesicles and turn out to be very stable over the simulation run time. The dynamic protocols employed in this study will facilitate further exploration of the sparsely studied, out-of-equilibrium dynamically trapped states in the shape space of the vesicle.

The appearance of distinct deformation patterns over the originally spherical vesicles under different dehydration rates is analogous to the formation of topological defects in the two-dimensional *XY* model at different quench rates from high to low temperatures. Both emergent structures of the flat areas over vesicles and topological defects among the ordered phase in the *XY* model provide the mechanism to break the continuous symmetry. In the two-dimensional *XY* model, it has been shown that the topological defect density follows a dynamic scaling law resulting from the balance of the quench rate and the relaxation dynamics of the system.[38−40] We therefore speculate that the appearance of flat areas and their coalescence over a continuously dehydrated crystalline vesicle may also be governed by a simple dynamic scaling law.

CONCLUSION

In summary, by using large-scale explicit-solvent CGMD simulations supplemented with analytical elasticity analysis, this study demonstrates that by dynamically changing vesicle volume we can controllably obtain a series of stable dynamically trapped shapes for both fluid and crystalline vesicles. Remarkably, simulations reveal that under protocol *M* (that is, to remove water massively) the morphology of the crystalline vesicle features emergent small flat areas across the vesicle, and their coalescence ultimately leads to the formation of various faceted polyhedral shapes. We propose the elastic free energy model and show that the crystalline nature of the vesicle is responsible for these deformation patterns. While faceted vesicles have been created on multicomponent vesicles[41] and liquid-crystal vesicles,[23] the dynamical protocol proposed in this work represents a new path for generating faceted shapes without introducing other structures. The tested concept of designing dynamic protocols to extend the shape space of both fluid and crystalline vesicles beyond the equilibrium zone may provide guidelines for vesicle geometry design in experiments for desired applications.

METHODS

Our previous simulation work has shown that typical ionic amphiphiles, such as −1 palmitic acid (C_{15}−COOH) and +3 trilysine (C_{16}−K_3), can spontaneously form hollow vesicle structures in aqueous environments, including experimentally observed faceted vesicles.[31] By dynamically changing the volume, these vesicles may exhibit even richer morphologies. The technique of explicit-solvent CGMD simulations provides an excellent tool for addressing this question. Using −1 palmitic acid (C_{15}−COOH) and +3 trilysine (C_{16}−K_3) as the building blocks, we constructed an electroneutral model system with an average ionization of 30% in the palmitic acid molecules, leading to the pH value of about 4.[31] The elementary ionic amphiphiles were numerically observed to form bilayer, spherical vesicles filled with water. The melting temperature for such bilayer membrane was experimentally measured to be around 328 K.[31] We performed simulations at the temperatures of 350 and 300 K and numerically observed the self-assembly of vesicles in fluid and crystalline states, suggesting the reliability of our simulations. The numerically synthesized vesicles were polydisperse in size as in experiments.[31,36,42] The value for the outer diameter ranged from 28 nm (containing 1000 +3 lipids, 3000 −1 lipids, and 7000 neutral lipids) to 52 nm (with the number of lipids quadrupled). For the limited size of the simulated system, we worked in a relatively high ion concentration of 2 M NaCl. A test for a given size vesicle of 50% ionization with counterions (Na^+) did not show appreciable shape shift (discussed below). A salient feature of these synthesized vesicles was that water molecules could permeate through them by thermal fluctuations.[43] An imposed osmotic pressure across the membrane especially sped up the flow of water molecules, leading to an appreciable change of the vesicle's volume and to the morphological transformation observed in experiments.[8,44]

We changed the volume of the vesicle by explicitly removing the water inside at different rates. New series of shapes not accessible *via* thermal equilibrations were produced in a controllable fashion. The resultant variety of morphologies represents rich potential metastable vesicle states, which we accessed *via* distinct dynamic protocols. A similar methodology to obtain various phase behaviors has been applied to polymer systems by choosing different annealing protocols. Here, to enlarge the shape space of both fluid and crystalline ionic vesicles, we have designed two distinct dynamic protocols for dehydrating the vesicle: incrementally and massively, dubbed *I* and *M*, respectively. Specifically, in *I*, 10% of the water inside the vesicle was removed in each step, and the relaxed vesicle shape was used as the initial state for the next step until the amount of removed water reached some preset value. In contrast, in *M*, a given amount of water was removed directly. In both procedures, the water inside the vesicle was uniformly removed to closely mimic the osmotic permeation in experiments and to avoid any uncontrollable buckling of the vesicle. For both fluid and crystalline vesicles, we numerically observed that *I* and *M* led to completely different series of stable vesicle shapes. Some of these shapes overlap with those found in previous experiments,[13] theory,[17,18] and simulations,[21,22] suggesting the reliability of our simulation model.

It is noteworthy that in the present work we remove the water molecules uniformly from the whole inner water volume. This operation corresponds to the regime where the flow of bulk water inside the vesicle can catch the rate of the water permeation very well through the vesicle wall. This is true if the permeation occurs sufficiently slowly. In this way, the bilayer membrane can be relaxed with the motion of inner water. In fact, uniformly dehydrating a fluid vesicle in our simulation can reproduce experimental shapes on the same condition. If we remove the surface part of the inner water volume there will be a vacuum bubble near the bilayer wall that will induce a sudden collapse and even rupture (for sufficiently large vesicle and bubble size) of the vesicle. The flow of the bulk water is not fast enough to relax the deformation of the vesicle. As a test, we selected a vesicle (diameter R = 28 nm, T = 300 K) and directly removed the surface water of the inner water volume (50% removed). We found that the shape is cubic rather than tetrahedral obtained by uniformly removing water, shown in Figure 7. Therefore, such a new way to remove water can lead to distinct deformation modes. There are also other methods to remove the inner water (*e.g.*, remove some local parts simultaneously) to reach different metastable states of the vesicle and create richer morphologies.

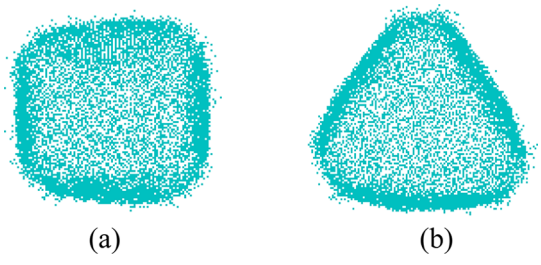

Figure 7. (a) With 50% surface water removed and (b) with 50% uniform water removed (diameter R = 28 nm, T = 300 K, and protocol *M*).

DOI: 10.1021/acsnano.5b06991
ACS Nano 2016, 10, 2287−2294

All molecular dynamic (MD) simulations were carried out using the Gromacs 4.6.5 software package,[45] and the MARTINI coarse-grained force field (version 2.1) was used.[46,47] The pressure (1 bar) and temperature were specified by the Berendsen method.[48] The periodic boundary conditions were applied in all directions. The MARTINI force field is generally based on the four-to-one mapping rule. That is, four heavy atoms are represented by one single interaction bead. Four interaction types (polar, intermediate polar, apolar, and charged) and some subtypes are classified according to the hydrogen-bonding capability or the degree of polarity. The mapping methodology for the present lipids can be found in our previous work.[31] For protocol *I*, we conducted a 100 ns MD run for each step, and the final state was used as the initial state of the next step. For the protocol *M*, we performed 200 ns MD run for each system. We checked the vesicle shape and potential energy to ensure that the vesicles reached stable states after dehydration.

AUTHOR INFORMATION

Corresponding Author

*E-mail: m-olvera@northwestern.edu.

Author Contributions

¶J.S. and Z.Y. contributed equally to this work.

Notes

The authors declare no competing financial interest.

ACKNOWLEDGMENTS

This work was supported by DOE-BES DE-FG02-08ER46539. J.S. would like to thank the National Natural Science Foundation of China (21574066). We would like to thank Baofu Qiao and Niels Boon for stimulating discussions.

REFERENCES

(1) Lipowsky, R.; Sackmann, E. Structure and Dynamics of Membranes: From Cells to Vesicles. *Handbook of Biological Physics*; Elsevier: Amsterdam, 1995; Vol. *1*, pp 1−1020.

(2) Noguchi, H.; Takasu, M. Self-Assembly of Amphiphiles into Vesicles: A Brownian Dynamics Simulation. *Phys. Rev. E: Stat. Phys., Plasmas, Fluids, Relat. Interdiscip. Top.* **2001**, *64*, 041913.

(3) Pornillos, O.; Ganser-Pornillos, B. K.; Kelly, B. N.; Hua, Y. Z.; Whitby, F. G.; Stout, D. C.; Sundquist, W. I.; Hill, C. P.; Yeager, M. X-Ray Structures of the Hexameric Building Block of the HIV Capsid. *Cell* **2009**, *137*, 1282−1292.

(4) Mayer, C.; Zaccarelli, E.; Stiakakis, E.; Likos, C. N.; Sciortino, F.; Munam, A.; Gauthier, M.; Hadjichristidis, N.; Iatrou, H.; Tartaglia, P.; Löwen, H.; Vlassopoulos, D. Asymmetric Caging in Soft Colloidal Mixtures. *Nat. Mater.* **2008**, *7*, 780−784.

(5) Uchegbu, I. F.; Vyas, S. P. Non-Ionic Surfactant Based Vesicles (Niosomes) in Drug Delivery. *Int. J. Pharm.* **1998**, *172*, 33−70.

(6) Dinsmore, A. D.; Hsu, M. F.; Nikolaides, M. G.; Marquez, M.; Bausch, A. R.; Weitz, D. A. Colloidosomes: Selectively Permeable Capsules Composed of Colloidal Particles. *Science* **2002**, *298*, 1006−1009.

(7) Versluis, F.; Tomatsu, I.; Kehr, S.; Fregonese, C.; Tepper, A. W. J. W.; Stuart, M. C. A.; Ravoo, B. J.; Koning, R. I.; Kros, A. Shape and Release Control of a Peptide Decorated Vesicle through pH Sensitive Orthogonal Supramolecular Interactions. *J. Am. Chem. Soc.* **2009**, *131*, 13186−13187.

(8) van der Heide, T.; Stuart, M. C. A.; Poolman, B. On the Osmotic Signal and Osmosensing Mechanism of an ABC Transport System for Glycine Betaine. *EMBO J.* **2001**, *20*, 7022−7032.

(9) Minkenberg, C. B.; Li, F.; van Rijn, P.; Florusse, L.; Boekhoven, J.; Stuart, M. C. A.; Koper, G. J. M.; Eelkema, R.; van Esch, J. H. Responsive Vesicles from Dynamic Covalent Surfactants. *Angew. Chem., Int. Ed.* **2011**, *50*, 3421−3424.

(10) Discher, D. E.; Eisenberg, A. Polymer Vesicles. *Science* **2002**, *297*, 967−973.

(11) Baumgart, T.; Hess, S. T.; Webb, W. W. Imaging Coexisting Fluid Domains in Biomembrane Models Coupling Curvature and Line Tension. *Nature* **2003**, *425*, 821−824.

(12) Datta, S. S.; Kim, S. H.; Paulose, J.; Abbaspourrad, A.; Nelson, D. R.; Weitz, D. A. Delayed Buckling and Guided Folding of Inhomogeneous Capsules. *Phys. Rev. Lett.* **2012**, *109*, 134302.

(13) Sakashita, A.; Urakami, N.; Ziherl, P.; Imai, M. Three-Dimensional Analysis of Lipid Vesicle Transformations. *Soft Matter* **2012**, *8*, 8569−8581.

(14) Seifert, U. Configurations of Fluid Membranes and Vesicles. *Adv. Phys.* **1997**, *46*, 13−137.

(15) Yong, E. H.; Nelson, D. R.; Mahadevan, L. Elastic Platonic Shells. *Phys. Rev. Lett.* **2013**, *111*, 177801.

(16) Vernizzi, G.; Sknepnek, R.; Olvera de la Cruz, M. Platonic and Archimedean Geometries in Multicomponent Elastic Membranes. *Proc. Natl. Acad. Sci. U. S. A.* **2011**, *108*, 4292−4296.

(17) Seifert, U.; Berndl, K.; Lipowsky, R. Shape Transformations of Vesicles: Phase Diagram for Spontaneous- Curvature and Bilayer-Coupling Models. *Phys. Rev. A: At., Mol., Opt. Phys.* **1991**, *44*, 1182−1202.

(18) Miao, L.; Seifert, U.; Wortis, M.; Döbereiner, H. G. Budding Transitions of Fluid-Bilayer Vesicles: The Effect of Area-Difference Elasticity. *Phys. Rev. E: Stat. Phys., Plasmas, Fluids, Relat. Interdiscip. Top.* **1994**, *49*, 5389−5407.

(19) Markvoort, A. J.; van Santen, R. A.; Hilbers, P. A. J. Vesicle Shapes from Molecular Dynamics Simulations. *J. Phys. Chem. B* **2006**, *110*, 22780−22785.

(20) Markvoort, A. J.; Spijker, P.; Smeijers, A. F.; Pieterse, K.; van Santen, R. A.; Hilbers, P. A. J. Vesicle Deformation by Draining: Geometrical and Topological Shape Changes. *J. Phys. Chem. B* **2009**, *113*, 8731−8737.

(21) Yuan, H. Y.; Huang, C. J.; Zhang, S. L. Dynamic Shape Transformations of Fluid Vesicles. *Soft Matter* **2010**, *6*, 4571−4579.

(22) Li, X. J. Shape Transformations of Bilayer Vesicles from Amphiphilic Block Copolymers: A Dissipative Particle Dynamics Simulation Study. *Soft Matter* **2013**, *9*, 11663−11670.

(23) Xing, X. J.; Shin, H.; Bowick, M. J.; Yao, Z. W.; Jia, L.; Li, M. H. Morphology of Nematic and Smectic Vesicles. *Proc. Natl. Acad. Sci. U. S. A.* **2012**, *109*, 5202−5206.

(24) Hirst, L. S.; Ossowski, A.; Fraser, M.; Geng, J.; Selinger, J. V.; Selinger, R. L. B. Morphology Transition in Lipid Vesicles Due to in-Plane Order and Topological Defects. *Proc. Natl. Acad. Sci. U. S. A.* **2013**, *110*, 3242−3247.

(25) Yong, E. H.; Nelson, D. R.; Mahadevan, L. Elastic Platonic Shells. *Phys. Rev. Lett.* **2013**, *111*, 177801.

(26) Sknepnek, R.; Vernizzi, G.; Olvera de la Cruz, M. Shape Change of Nanocontainers *via* a Reversible Ionic Buckling. *Phys. Rev. Lett.* **2011**, *106*, 215504.

(27) Jadhao, V.; Yao, Z. W.; Thomas, C. K.; Olvera de la Cruz, M. Coulomb Energy of Uniformly-Charged Spheroidal Shell Systems. *arXiv:1501.03582* **2015**.

(28) Schneider, S.; Gompper, G. Shapes of Crystalline Domains on Spherical Fluid Vesicles. *Europhys. Lett.* **2005**, *70*, 136−142.

(29) Yao, Z. W.; Olvera de la Cruz, M. Topological Defects in Flat Geometry: The Role of Density Inhomogeneity. *Phys. Rev. Lett.* **2013**, *111*, 115503.

(30) Fan, C. G.; Cheng, S. Q.; Liu, Y.; Escobar, C. M.; Crowley, C. S.; Jefferson, R. E.; Yeates, T. O.; Bobik, T. A. Short N-Terminal Sequences Package Proteins into Bacterial Microcompartments. *Proc. Natl. Acad. Sci. U. S. A.* **2010**, *107*, 7509−7514.

(31) Leung, C. Y.; Palmer, L. C.; Qiao, B. F.; Kewalramani, S.; Sknepnek, R.; Newcomb, C. J.; Greenfield, M. A.; Vernizzi, G.; Stupp, S. I.; Bedzyk, M. J.; Olvera de la Cruz, M. Molecular Crystallization Controlled by pH Regulates Mesoscopic Membrane Morphology. *ACS Nano* **2012**, *6*, 10901−10909.

(32) Yong, E. H.; Nelson, D. R.; Mahadevan, L. Elastic Platonic Shells. *Phys. Rev. Lett.* **2013**, *111*, 177801.

(33) Landau, L. D.; Lifshitz, E. M. *Theory of Elasticity*; Butterworth Heinemann, 1986; Vol. *7*, pp 1−195.

DOI: 10.1021/acsnano.5b06991
ACS Nano 2016, 10, 2287−2294

(34) Pabst, G.; Kučerka, N.; Nieh, M. P.; Rheinstädter, M. C.; Katsaras, J. Applications of Neutron and X-Ray Scattering to the Study of Biologically Relevant Model Membranes. *Chem. Phys. Lipids* **2010**, *163*, 460−479.
(35) Nelson, D.; Weinberg, S.; Piran, T. *Statistical Mechanics of Membranes and Surfaces*; World Scientific, 2004; pp 1−444.
(36) Leung, C. Y.; Palmer, L. C.; Kewalramani, S.; Qiao, B. F.; Stupp, S. I.; Olvera de la Cruz, M.; Bedzyk, M. J. Crystalline Polymorphism Induced by Charge Regulation in Ionic Membranes. *Proc. Natl. Acad. Sci. U. S. A.* **2013**, *110*, 16309−16314.
(37) Zhong-can, O.-Y.; Helfrich, W. Bending Energy of Vesicle Membranes: General Expressions for the First, Second, and Third Variation of the Shape Energy and Applications to Spheres and Cylinders. *Phys. Rev. A: At., Mol., Opt. Phys.* **1989**, *39*, 5280−5288.
(38) Bray, A. J.; Rutenberg, A. D. Growth Laws for Phase Ordering. *Phys. Rev. E: Stat. Phys., Plasmas, Fluids, Relat. Interdiscip. Top.* **1994**, *49*, R27−R30.
(39) Rutenberg, A. D.; Bray, A. J. Energy-Scaling Approach to Phase-Ordering Growth Laws. *Phys. Rev. E: Stat. Phys., Plasmas, Fluids, Relat. Interdiscip. Top.* **1995**, *51*, 5499−5514.
(40) Rojas, F.; Rutenberg, A. D. Dynamical Scaling: The Two-Dimensional XY Model Following a Quench. *Phys. Rev. E: Stat. Phys., Plasmas, Fluids, Relat. Interdiscip. Top.* **1999**, *60*, 212−221.
(41) Sknepnek, R.; Olvera de la Cruz, M. Nonlinear Elastic Model for Faceting of Vesicles with Soft Grain Boundaries. *Phys. Rev. E* **2012**, *85*, 050501(R).
(42) Greenfield, M. A.; Palmer, L. C.; Vernizzi, G.; Olvera de la Cruz, M.; Stupp, S. I. Buckled Membranes in Mixed-Valence Ionic Amphiphile Vesicles. *J. Am. Chem. Soc.* **2009**, *131*, 12030−12031.
(43) Qiao, B. F.; Olvera de la Cruz, M. Driving Force for Water Permeation Across Lipid Membranes. *J. Phys. Chem. Lett.* **2013**, *4*, 3233−3237.
(44) Yanagisawa, M.; Imai, M.; Taniguchi, T. Shape Deformation of Ternary Vesicles Coupled with Phase Separation. *Phys. Rev. Lett.* **2008**, *100*, 148102.
(45) van der Spoel, D.; Lindahl, E.; Hess, B.; Groenhof, G.; Mark, A. E.; Berendsen, H. J. C. GROMACS: Fast, Flexible and Free. *J. Comput. Chem.* **2005**, *26*, 1701−1718.
(46) Monticelli, L.; Kandasamy, S. K.; Periole, X.; Larson, R. G.; Tieleman, D. P.; Marrink, S. J. The MARTINI Coarse Grained Force Field: Extension to Proteins. *J. Chem. Theory Comput.* **2008**, *4*, 819−834.
(47) Marrink, S. J.; de Vries, A. H.; Mark, A. E. Coarse Grained Model for Semiquantitative Lipid Simulations. *J. Phys. Chem. B* **2004**, *108*, 750−760.
(48) Berendsen, H. J. C.; Postma, J. P. M.; van Gunsteren, W. F.; DiNola, A.; Haak, J. R. Molecular dynamics with coupling to an external bath. *J. Chem. Phys.* **1984**, *81*, 3684−3690.

NOTE ADDED AFTER ASAP PUBLICATION

This paper posted ASAP on 1/26/16. Due to a production error, equations were corrected in the Results and Discussion section and the revised version was reposted on 1/28/16.

DOI: 10.1021/acsnano.5b06991
ACS Nano 2016, 10, 2287−2294